Basic studies of ductile failure processes and implications for fracture prediction

J. ZUO, M. A. SUTTON and X. DENG

Department of Mechanical Engineering, University of South Carolina, Columbia, SC 29208, USA

Received in final form 6 October 2003

ABSTRACT Fracture of ductile materials has frequently been observed to result from the nucleation, growth and coalescence of microscopic voids. Experimental and analytical studies have shown that both the stress constraint factor and the effective plastic strain play a significant role in the ductile failure process. Experimental results also suggest that these two parameters are not independent of each other at failure initiation. In this study, a methodology for characterizing the effect of stress constraint A_m (which is defined to be the ratio of the mean stress and the effective stress $A_m = \sigma_m/\sigma_e$) on ductile failure is proposed. This methodology is based on experimental evidence that shows the effective plastic strain at failure initiation has a one-to-one relationship with stress constraint. Numerical analyses based on plane strain and three-dimensional unit-cell models have been carried out to investigate failure initiation of the unit cell under different constraint conditions. Results from the numerical studies indicate (a) for each void volume fraction, there exists a local failure locus in terms of mesoscopic quantities, σ_m and σ_e, that adequately predict incipient local micro-void link-up, (b) the results are fully consistent with a failure criterion that maximizes mesoscopic effective stress for a constant level of stress constraint A_m, (c) for high to moderate constraint A_m, the link-up envelope values for σ_m and σ_e are consistent with limit load conditions where the critical principal stress σ_{1c} corresponds to the maximum principal stress in the loading history and (d) for low constraint, the link-up envelope values for σ_m and σ_e correspond to link-up conditions having high levels of plastic strain and a principal stress σ_1 that is lower than the maximum value for this loading history. Thus, the results suggest that a two-parameter ductile fracture criterion is plausible, such as critical crack opening displacement (COD) and stress constraint A_m, for predicting the process of stable tearing in materials undergoing ductile void growth during the fracture process.

Keywords ductile fracture criterion; stress constraint; void volume fraction.

INTRODUCTION

Ductile fracture of metals and metallic alloys has been observed to be the result of nucleation, growth and coalescence of microscopic voids. So far, two major approaches used to study ductile fracture of materials have been addressed in the literature. One approach utilizes the macroscopic crack tip parameters (e.g., the J-Integral,[1] the HRR singular fields,[2,3] mixed-mode COD,[4] J-A_2[5]) to predict crack growth. Another approach is based on the constitutive model initially proposed by Gurson,[6] and improved and extended by Needleman and Tvergaard[7] to account for the rapid loss of carrying capacity during void coalescence by incorporating the effects of void nucleation, growth and coalescence. This modified Gurson's model was also implemented into constitutive equations for porous compressible material and used to predict the softening and maximum load behaviour with a semiimplicit integration algorithm.[8,9] To simulate the process of crack growth in ductile materials using the modified Gurson's model, a computational cell methodology was developed,[10–13] in which special cell elements were arranged along a prospective crack path.

In the modified Gurson's model, it was postulated that failure occurs when the void volume fraction reaches its

Correspondence: M.A. Sutton. E-mail: sutton@sc.edu

ultimate value f_u. In other words, the ultimate void volume fraction f_u defined by Tvergaard and Needleman[14–16] refers to the case in which the macroscopic stress carrying capacity vanishes. In order to match experimental results, three parameters q_1, q_2 and q_3 were introduced in the model. The model was shown to be able to give an adequate representation of experimental results[16] when $q_1 = q_3 = 1.5$ and $q_2 = 1$, which include predicting the effect of softening due to void coalescence. From this modified Gurson's model, one can obtain that $f_u = 1/q_1$. However, physical measurements noted by Thomason[17] clearly show that the high porosity levels inherent to this model for termination of ductile plastic flow at realistic fracture strains are nearly impossible. For this reason, it is unclear whether the proper void-coalescence behaviour is captured in this model.

Most of the literature based on the Gurson's model focuses on the study of material behaviour under the consideration of spherical void growth and coalescence. In order to capture the effect of void shape (void aspect ratio) on the onset of void coalescence, an extended model for axisymmetric void growth and coalescence was proposed through the numerical study of a representative volume element (RVE).[18] For the same purpose, an extended Gurson's model for void coalescence in periodically voided ductile solids was proposed.[19–21] In this model a cylindrical RVE containing an initially spherical void and subjected to axisymmetric loading was employed and void coalescence was assumed to correspond to a sudden concentration of the deformation in the RVE. The extended Gurson's model has shown the potential for improved accuracy in the prediction of void growth and coalescence.

Previous studies of ductile fracture[22–24] show that the main macroscopic parameters influencing microscopic void nucleation, growth and coalescence, and hence ductile fracture, are the stress constraint factor, A_m, and the effective plastic strain, where the stress constraint factor A_m is defined as the ratio of the hydrostatic mean stress σ_m to the von Mises effective stress σ_e (i.e., $A_m = \sigma_m/\sigma_e$). Hancock and Mackenzie[23] experimentally studied the mechanisms of ductile failure in high-strength steels subjected to multiaxial stress states and evaluated the effect of the stress constraint factor on the average plastic strain at failure initiation from the Bridgman's equation. Their results indicate that notched specimens in three low-alloy steels have a critical effective plastic strain, ε_{pc}, at failure initiation that is a monotonically decreasing function of the level of A_m. Subsequently, Walsh *et al.*[24] investigated the ductile fracture of 2134 type Al alloys and observed that the material's rupture ductility decreases as A_m increases. Figure 1 shows a typical experimental relationship between the critical effective plastic strain and the stress constraint, which indicates that the rupture ductility (represented by the critical effective plastic strain) decreases

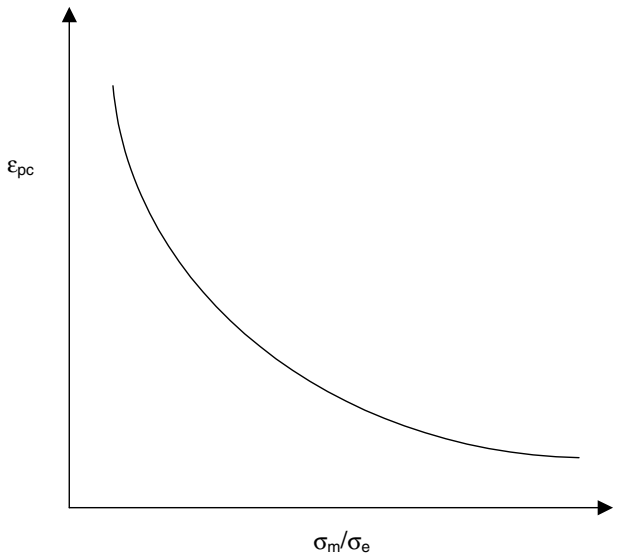

Fig. 1 Typical relationship between critical plastic strain and constraint.

monotonically as the level of stress constraint A_m increases. For a given stress state, ε_{pc}, is uniquely determined by the ε_{pc}–σ_m/σ_e relationship. In this regard, numerical results indicate that the stress constraint plays a key role in the ductile–brittle transition in small scale yielding.[25] Furthermore, recent numerical studies for voided materials have shown that the relationship of macroscopic effective stress σ_e to macroscopic effective plastic strain E_p will be a function of the stress constraint A_m.[26]

A recent comprehensive review paper on ductile fracture modelling by Thomason,[17] which utilizes extensive experimental, theoretical and computational results obtained both by the author and recognized researchers throughout the world, provides a clear framework for ductile fracture modelling. In his work, Thomason provides convincing evidence that (a) crack extension during the void-coalescence process is by inter-void matrix failure at limit load, (b) the dilatational plastic void-growth model of ductile fracture,[14–16] which predicts the presence of large voids, is inconsistent with SEM and microstructural observations of ductile fracture that show numerous small voids throughout the fracture surface and (c) uniqueness issues in numerical simulations of the void coalescence process (which may arise due to the plastic velocity field) may limit the applicability of finite element methods.

Utilizing the experimental and analytical work noted above, and by making use of a unit cell finite element model, the present work will show that two parameters—the *stress constraint factor*, $A_m = \sigma_m/\sigma_e$, and the *critical effective plastic strain*, ε_{pc}—provide the basis for developing a framework to characterize the effect of stress constraint A_m on local ductile failure of materials. In the remainder of

this paper, the following section describes detailed numerical analyses based on two-dimensional plane strain and three-dimensional unit-cell finite element models, with an emphasis on identifying cell-level stress quantities capable of predicting the link-up of neighbouring voids. In section 'Numerical Simulation Results', results from the unit-cell analyses are presented. In section 'A Criterion for Predicting Void Link-Up' and the Appendix, the results in following two sections are shown to be consistent with (a) the σ_m/σ_e and ε_{pc} relationship in Fig. 1 and (b) a local void link-up model, $F(\sigma_m, \sigma_e, f_0)$, where f_0 is the initial void volume fraction. The results from the numerical simulations indicate that, at the instant of local void link-up, (a) the effective stress reaches its maximum under constant constraint loading conditions and (b) the majority of the σ_m–σ_e loci at the instant of local failure are consistent with a local limit load failure criterion. 'A Criterion for Predicting Void Link-Up' section also presents a detailed discussion of the results, along with comparisons to appropriate existing literature. The 'Discussion of Results' and 'Additional Remarks' sections present concluding remarks.

FINITE ELEMENT BASED, UNIT-CELL MODEL FOR VOID LINK-UP STUDIES

Two- and three-dimensional unit-cell models used in this study are shown in Figs 2–4. The void in each of the models has an initial void volume fraction f_0. The average strain rate on a voided region, as in Bishop and Hill,[27] is defined in terms of the velocity field on the outer surface of a unit-cell model, as given below

$$\dot{\varepsilon}_{ij} = \frac{1}{V}\int_A \frac{1}{2}\left(\dot{u}_i n_j + \dot{u}_j n_i\right) \mathrm{d}A, \tag{1}$$

where V is the total volume of a unit-cell model (matrix + void), A is the total outer surface of the model, $\dot{u}_i$ is the rate of displacement (velocity) applied on the outer

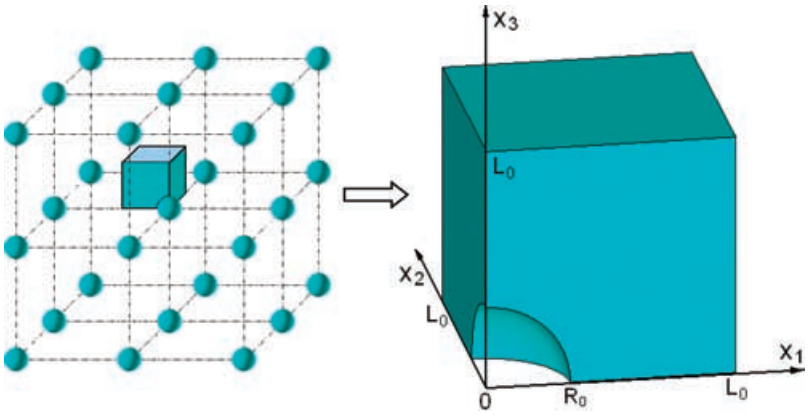

Fig. 2 Three-dimensional periodic array of voids and unit cell material model.

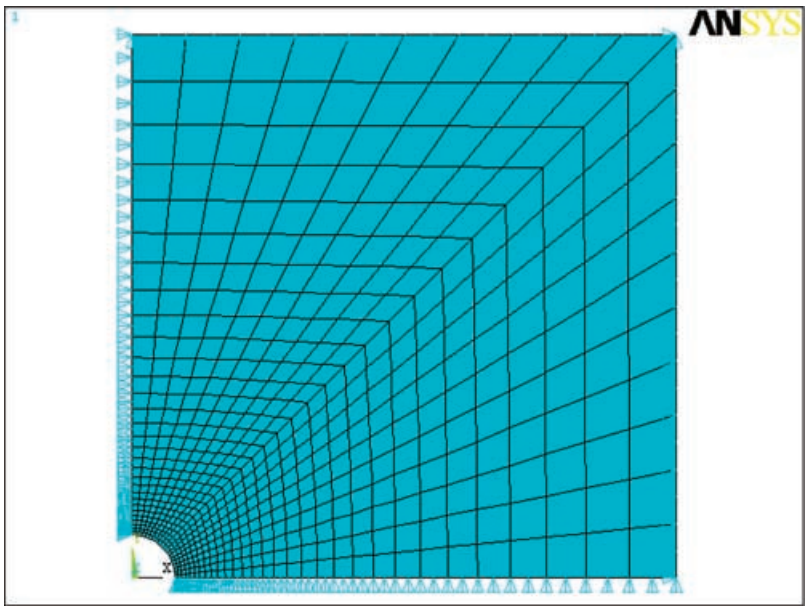

Fig. 3 One-quarter model for 2D plane strain unit cell.

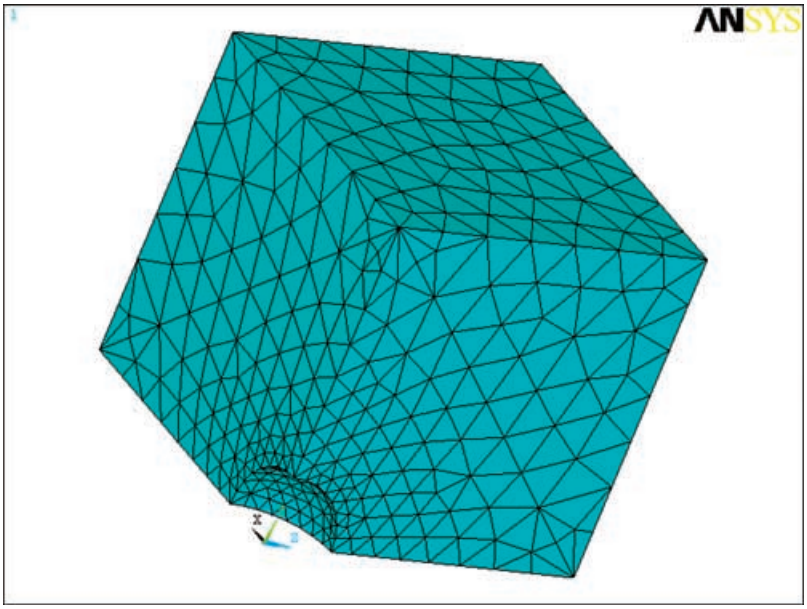

Fig. 4 One-eighth model for 3D unit cell.

surface of the model and n_i is the unit outward normal on A. In all calculations, V and A are referred to the deformed configuration. The average stress components in a voided region are defined and computed by integration over the appropriate faces of the unit-cell model as follows

$$\sigma_{ij} = \frac{1}{A}\int_A T_{ij}\,dA. \tag{2}$$

The matrix of the unit-cell model of a porous ductile solid to be studied here, as shown in Fig. 2 for a three-dimensional periodic array of spherical microvoids, is defined as a strain-hardening elastic–plastic material, described by Eq. (3).

$$\varepsilon = \begin{cases} \dfrac{\sigma}{E} & \text{for} \quad \sigma \le \sigma_y \\ \dfrac{\sigma_y}{E}\left(\dfrac{\sigma}{\sigma_y}\right)^n & \text{for} \quad \sigma > \sigma_y \end{cases} \tag{3}$$

where σ_y is the initial uniaxial yield stress, E is the Young's modulus and n is the strain hardening exponent. Properties for the matrix material used in this work are that $\sigma_y = 360$ MPa, $E = 71.2$ GPa and $n = 7.4$.

Figures 3 and 4 show, respectively, a one-quarter, two-dimensional plane strain model and a one-eighth, three-dimensional model for a unit cell ($L_0 = 1$). In this work, initial void volume fractions in the range $0.00125 < f_0 < 0.0800$ were modelled by varying the radius of the void, R_0, in a unit cell.

All 2D and 3D analyses were performed using (a) the commercial code, ANSYS, Version 5.6, and (b) the large deformation formulation in ANSYS for both rotations and strains. The implicit finite element model and incremental plasticity theory were employed in all numerical calculations.

Convergence of the finite element results was investigated for the element size and distribution in the computational cell. Tolerances used in ANSYS to determine convergence of the solution during the loading process were set at 0.0001 for the ratio of the residual in total force (moment) to the total force (moment). The maximum size of strain steps during the incremental loading is controlled to less than 0.0125. The convergence studies indicate that a total of 600, eight-node plane strain elements having 1901 nodes are required for the 2D model and a total of 3740, 10-node tetrahedral elements with 6426 nodes are sufficient for the 3D analyses.

Boundary conditions for the analysis include (a) symmetry displacement conditions along the symmetry surfaces (e.g., for 3D the conditions are $u_{x1} = 0$ in plane of $x_1 = 0$, $u_{x2} = 0$ in plane of $x_2 = 0$, $u_{x3} = 0$ in plane of $x_3 = 0$) and (b) uniform displacement loading along remaining surfaces (e.g., for 3D the conditions are $u_{x1} = C_{x1}$ in plane of $x_1 = L_o$, $u_{x2} = C_{x2}$ in plane of $x_2 = L_o$, $u_{x3} = C_{x3}$ in plane of $x_3 = L_o$, where L_o is the size of the unit cell). By varying the values for C_{x1}, C_{x2} and C_{x3}, the values of σ_m, σ_e and A_m applied to the unit cell are computed by (a) integrating the tractions on the surfaces $x_i = L_o$ ($i = 1$, 2 and 3) to obtain the force vectors, (b) computing the average surface stresses using the surface areas and Eq. (2) and (c) using the resulting stresses to determine the average applied values for σ_m, σ_e and A_m. The values for the applied stresses varied over a wide range given by the following inequalities:

- $0 < \sigma_m < 1200$ Mpa
- 50 Mpa $< \sigma_e <$ 590 Mpa
- $0 < A_m = \sigma_m/\sigma_e < 10$.

Each finite element analysis is performed under displacement control. The boundaries are displaced uniformly and monotonically throughout the loading process. In addition, all displacements are increased in the same proportion throughout the loading process.

In this study, void link up is investigated by considering all situations in which the plastic zone in a unit cell extends from the void boundary to the boundary of the exterior unit cell walls. Thus, link-up is said to have occurred when the contour, at a specified level, of the effective plastic strain in the matrix, $\varepsilon_p = (\frac{2}{3}\varepsilon_{ij}^p \varepsilon_{ij}^p)^{1/2}$ (where ε_{ij}^p is the plastic strain tensor and the summation convention is assumed), intersects both the void boundary and a symmetry boundary of the unit cell. For each pre-specified level of the effective plastic strain, our analyses indicated that different results are predicted to occur at void link-up as the level of stress constraint A_m changes; variations in A_m can be achieved by manipulating the applied displacement boundary conditions. Experimental studies[23,24] show that the critical effective plastic strain is a monotonic function of the stress constraint A_m. In other words, for each prespecified level of effective plastic strain, only one level of stress constraint A_m in these calculations corresponds to conditions that result in actual void link-up (further discussion related to this issue is given in appendix).

To determine when a contour having the pre-specified ε_p continuously extends between the void boundary and the neighbouring region, the solution at incremental displacement steps is stored and evaluated during post-processing. By symmetry, the contour also will extend to each neighbouring void. Once the appropriate loading step is determined, the average applied values for all stress components at incipient void link-up are computed, including σ_m, σ_e and A_m.

For cases approaching the pure shear situation (in which $A_m \to 0$), it is noted that large void distortions will occur, resulting in the collapse of the void during the loading process. In these cases, localization of the effective plastic strain was observed along a well-defined direction and link-up was defined in the manner noted above. Because void boundary contact was not considered in our analysis, it is important to note that (a) void boundary contact only occurs at low constraint and (b) link-up occurs prior to void boundary contact for almost all of the low constraint cases ($A_m \geq 0.01$) considered. For those few cases where void contact occurred prior to link-up conditions, our studies indicate that using contact to define link-up would have negligible effect on the results.

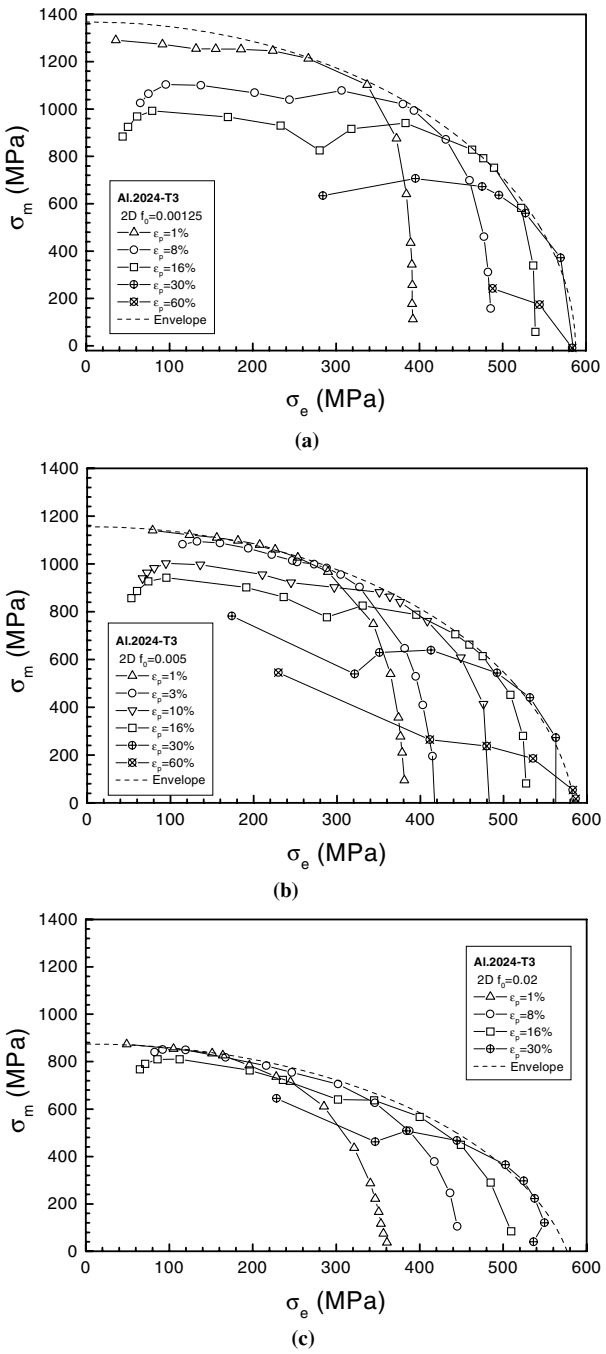

Fig. 5 Two-dimensional simulation results at void link-up for (a) $f_0 = 0.00125$; (b) $f_0 = 0.005$ (c) $f_0 = 0.020$.

NUMERICAL SIMULATION RESULTS

For specific values of the link-up effective plastic strain, ε_p, and a range of applied displacement boundary conditions, Figs 5 and 6 show the values of (σ_m, σ_e) that were applied to the region at link-up for (a) 2D plane strain and $f_0 = 0.00125$, 0.005 and 0.020 and (b) 3D conditions and $f_0 = 0.005$, 0.020 and 0.080.

As is apparent in the numerical results shown in Figs 5 and 6, for each ε_p there are several values of (σ_m, σ_e) obtained by the simulations that result in 'link-up' to the

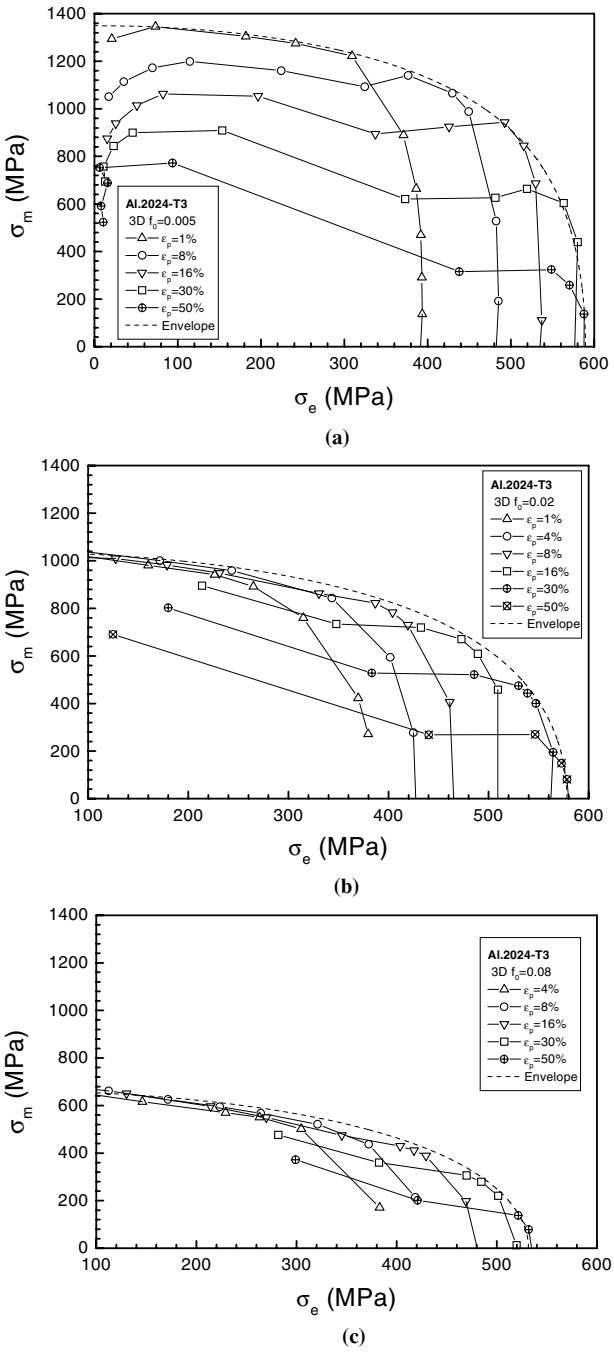

Fig. 6 Three-dimensional simulation results at void link-up for (a) $f_0 = 0.005$; (b) $f_0 = 0.020$ (c) $f_0 = 0.080$.

neighbouring void. Because previous experimental evidence (Fig. 1) suggests that a unique, monotonic relationship exists between A_m and ε_{pc} (the critical value of ε_p at ductile failure initiation), an approach is needed to determine whether the simulations contain the requisite information for predicting void link-up while simultaneously resulting in a monotonic A_m–ε_{pc} relationship.

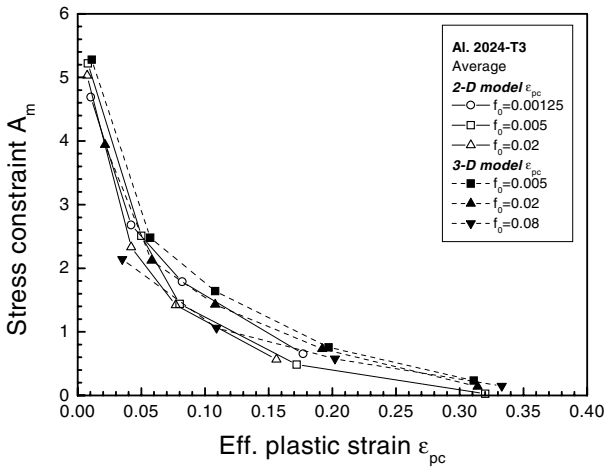

Fig. 7 A_m versus average effective plastic strain ε_{pc}.

Inspection of the data in Figs 5 and 6 suggests that the simulation results for each value of f_0 are bounded by an envelope, which is tangent to each of the ε_p curves. Note that each point on the envelope, say $(\sigma_m, \sigma_e)^i$, lies on one ε_p-curve and uniquely determines a stress constraint value, say A_m^i. One definition of the critical effective plastic strain (say ε_{pc}^i) corresponding to the stress constraint A_m^i would be the effective plastic strain for that ε_p-curve, which will be referred to as the *contour* ε_{pc} *value*. Alternatively, it is more consistent to use the averaged (homogenized) value of the effective plastic strain for the unit cell to define ε_{pc}^i, which is computed based on the displacement conditions applied at the unit cell boundaries and will be called the *average* ε_{pc} *value*.

The resulting relationship between the stress constraint A_m and the average critical effective plastic strain ε_{pc} for both the 2D and 3D unit cell models is shown in Fig. 7 based on the $(A_m^i, \varepsilon_{pc}^i)$ pair values defined earlier. For comparison, Figs 8a (for 2D unit cell) and b (for 3D unit cell) show the A_m–ε_{pc} relationship if ε_{pc} is defined as the average effective plastic strain or as the effective plastic strain along the contour that connects the outer surface of the cell to the void surface. The results in Figs 7 and 8 demonstrate that each envelope in Figs 5 and 6 corresponds to a monotonic relationship between A_m and ε_{pc}, which is fully consistent with experimental evidence such as shown in Fig. 1, in that ε_{pc} decreases as A_m increases.

A CRITERION FOR PREDICTING VOID LINK-UP

A brief summary of known properties of typical σ_e–ε_p relationships is presented in this section to provide a framework for understanding the envelope functions developed in the previous section.

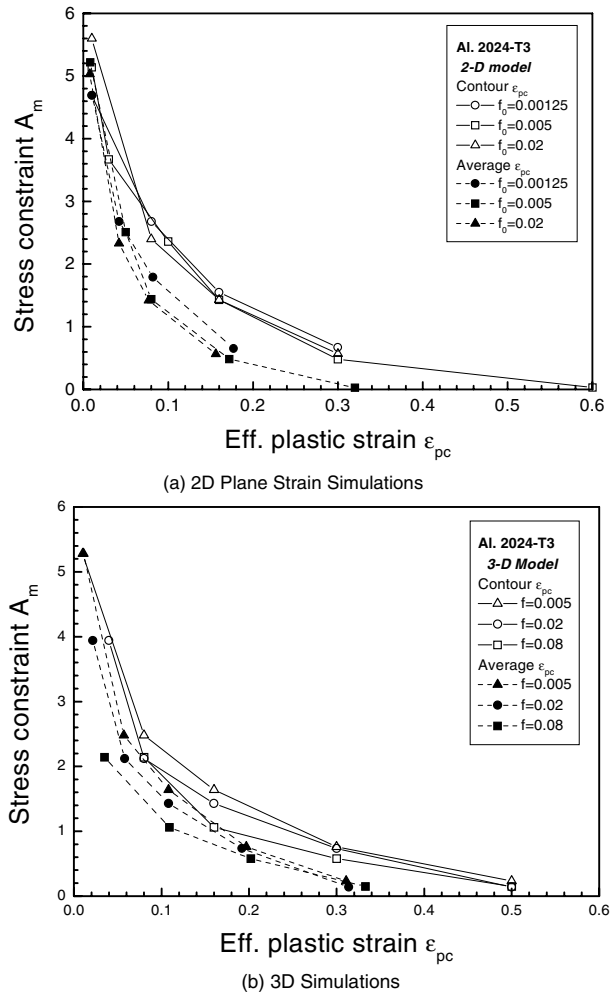

Fig. 8 Comparison of simulation results for ε_{pc}^{avg} versus A_m and $\varepsilon_{pc}^{contour}$ versus A_m (a) 2D simulations; (b) 3D simulations.

When $f_0 = 0$, the relationship between σ_e and ε_p is nearly independent of stress constraint A_m in many materials. If the effect of impurities and inclusion separation (especially under finite deformation) are considered, it is well know that the deformation response of porous material is a strong function of the level of stress constraint A_m. In such cases, volumetric deformation is dominant under high levels of stress constraint A_m and distortional deformation is dominant under low levels of stress constraint A_m. Thus, regions with microstructural material variations are expected to result in material response that changes with stress constraint A_m.

For a typical void volume fraction f_0 this is shown in Fig. 9 based on unit-cell results described in the preceding section. The effective stress–plastic strain relationship is a function of A_m and the response is assumed to be determined while maintaining a constant stress constraint, A_m, throughout the loading history. Note that, for each

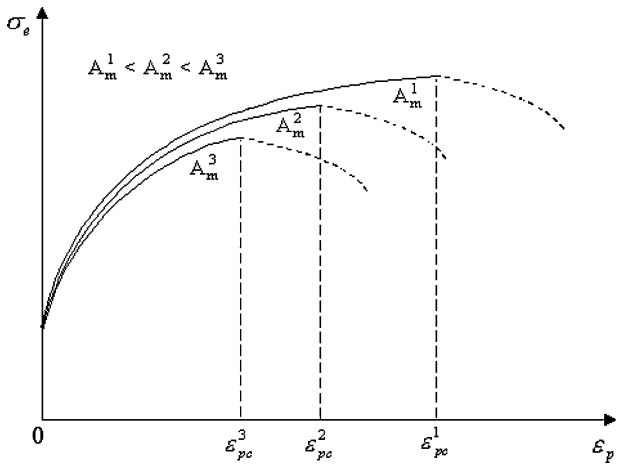

Fig. 9 σ_e versus ε_p as a function of A_m for a typical void volume fraction, f_0.

level of constraint, say A_m^i, the σ_e–ε_p relationship for a voided material is assumed to be monotonic up to σ_e^{max}, with the relationship being a function of A_m. This assumption, which is consistent with experimental evidence, is used in the attached appendix.

Furthermore, the *maximum in* σ_e–ε_p *for each* A_m is consistent with the numerical simulation results shown in 'Numerical Simulation Results' section. Specifically, for $\sigma_e = \sigma_e^{max}$, the values $(\sigma_m, \sigma_e, f_0)$ obtained for all A_m represent a function that corresponds to a monotonic relationship between ε_{pc} and A_m so that $A_m{}^1 < A_m{}^2 < A_m{}^3 \Rightarrow \varepsilon_{pc}{}^1 > \varepsilon_{pc}{}^2 > \varepsilon_{pc}{}^3$. These $(A_m^i, \varepsilon_{pc}^i)$ pairs (Fig. 9) are the same as those discussed in the preceding section.

The developments in the Appendix suggest that there are two interpretations of the proposed local void link-up criterion. First, for a given void volume fraction f_0, there exists a locus of values for (σ_m, σ_e) that correspond to local stress conditions resulting in void link-up, where the effective plastic strain at void link-up varies with the corresponding constraint, A_m.

Second, consistent with the discussion given above, it is shown that the locus of values for (σ_m, σ_e) is in accordance with the achievement of a maximum in the effective stress under a constant level of constraint, A_m. Considering the effective plastic strain corresponding to the maximum effective stress as the plastic strain at the initiation of void link-up for each level of constraint, then the effective plastic strain at void link-up under different stress constraint will decrease monotonically with increasing constraint. These concepts can be formulated into a void link-up criterion: '*Under a constant level of constraint*, A_m, *failure initiation occurs in a ductile material when the effective stress reaches its maximum in the loading history*'.

It is noted that this criterion is consistent with both experimental results[23,24] and numerical predictions.[26]

Furthermore, as is discussed in the appendix, it is possible to demonstrate that, if one assumes a one-to-one relationship $F(\varepsilon_{pc}, A_m, f_0)$ between the critical plastic strain in the remaining material and macroscopic stress constraint A_m such as shown in Figs 1, 7 and 8, then there exists a unique functional relationship $H(A_m, \sigma_e, f_0)$ at failure initiation. Conversely, it can be shown that if one assumes there exists a unique functional relationship $H(A_m, \sigma_e, f_0)$ at failure initiation and a monotonic relationship between ε_p and σ_e for each void volume fraction and constraint, then this implies a unique functional relationship $F(\varepsilon_{pc}, A_m, f_0)$ that is similar to the form shown in Fig. 1.

In the following section, results from detailed finite element studies of voided materials are presented which support the proposed link-up criterion.

DISCUSSION OF RESULTS

The envelope values for $(\sigma_m, \sigma_e, f_0)$ shown in Fig. 6 can be represented by the following least-squares formula:

$$\Phi(\sigma_e, \sigma_m, f_0) = \frac{\sigma_e^2}{\sigma_f^2} + C_2\frac{\sigma_m^2}{\sigma_f^2} + C_1\frac{\sigma_m}{\sigma_f} - C_0 = 0, \qquad (4)$$

in which σ_f is the true fracture stress in uniaxial tension, and C_0, C_1 and C_2 are constants. For Aluminium alloy 2024-T3, $\sigma_f = 570$ MPa and the constants are

$$C_0 = 1 - \tfrac{1}{2} f_0^{\frac{1}{3}}, \qquad (5)$$

$$C_1 = 28.5 f_0^2 + 3.14 f_0 - 0.0026, \qquad (6)$$

$$C_2 = 0.381 - 0.226\, e^{-62.7 f_0}. \qquad (7)$$

For the 3D simulations, the results given by Eq. (4) are shown in Fig. 10 for a range of initial void volume fractions, $0.001 < f_0 \leq 0.10$.

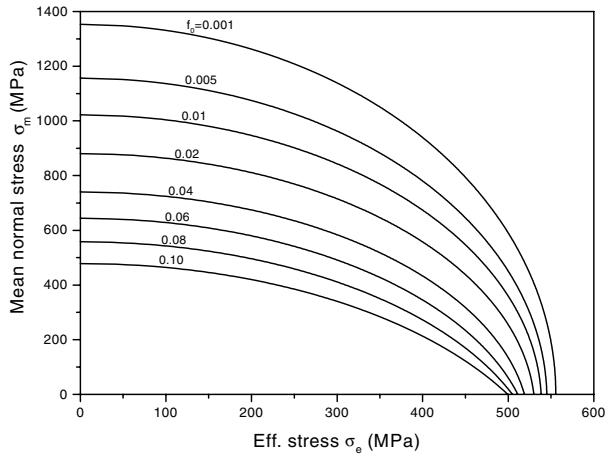

Fig. 10 Envelope functions σ_m and σ_e for each f_0.

With regard to the results in Fig. 10, the higher constraint regions correspond to link-up conditions along one of the axes, with a shape that is consistent with plane strain, mode I slip line fields. A typical shape for the region of plastic deformation obtained in these simulations is shown in Fig. 11.

In addition, the results from both 2D and 3D simulations indicate that the use of an effective plastic strain criterion for predicting link-up in regions of high to moderate constraint is fully consistent with a maximum load condition. That is, the average stress states in Fig. 10 required for void link-up in regions of high to moderate constraint correspond to the average stresses at *maximum load*. This observation is consistent with the work of Thomason[17] where he notes that plastic limit load failure of the inter-void matrix is the final stage of the process resulting in localized separation of the material.

Under low constraint conditions, link-up occurs along effective plastic strain contours at approximately 45° from the axes, with a shape that suggests plane stress conditions; a typical plastic zone obtained in these simulations under the condition of low constraint is shown in Fig. 12. In fact, our simulations indicate that the use of an effective plastic strain criterion for predicting link-up under low constraint conditions is consistent with a maximum effective stress condition. That is, the average stress states in Fig. 10 required for void link-up under low constraint have a maximum in the effective stress.

Though the stress states at link-up under low constraint conditions have a maximum in σ_e, the numerical results from both 2D plane strain and 3D simulations under low constraint conditions show that the corresponding loading is not a maximum in the loading history. In fact, the results shown that the applied load reaches its maximum and then decreases with increasing deformation of the cell model until void link-up occurs. In other words, the critical load corresponding to the stress states required for void link-up is less than the maximum load in the loading history under low constraint condition. In addition, the numerical results also show that the critical load defined at the instance of void link-up is dependent on both void volume fraction f_0 and constraint A_m under low constraint conditions.

The numerical results from both 2D and 3D simulations also indicate that the critical principal stress σ_{1c}, which corresponds to the critical load in our work, is a function of stress constraint A_m and void volume fraction f_0. Thus, there exists a function, $\sigma_{1c} = \sigma_{1c}(\varepsilon_{pc}, f_0)$ that can be established by using the relationship of the critical effective plastic strain ε_{pc} to constraint A_m; a typical relationship between σ_{1c} and ε_{pc} for ductile materials is shown in Fig. 13. As can be seen, the critical principal stress σ_{1c} decreases with increasing critical effective plastic strain. The relationship shown in Fig. 13 is in agreement with

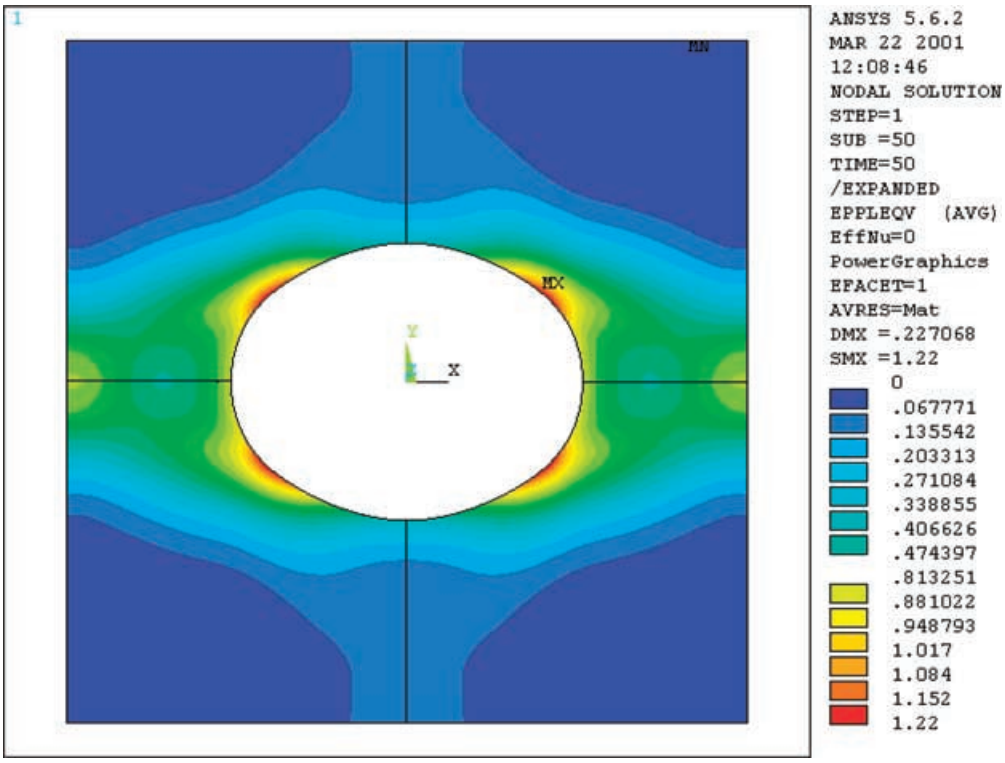

Fig. 11 Typical shape of plastic zone at link-up for high to moderate constraint.

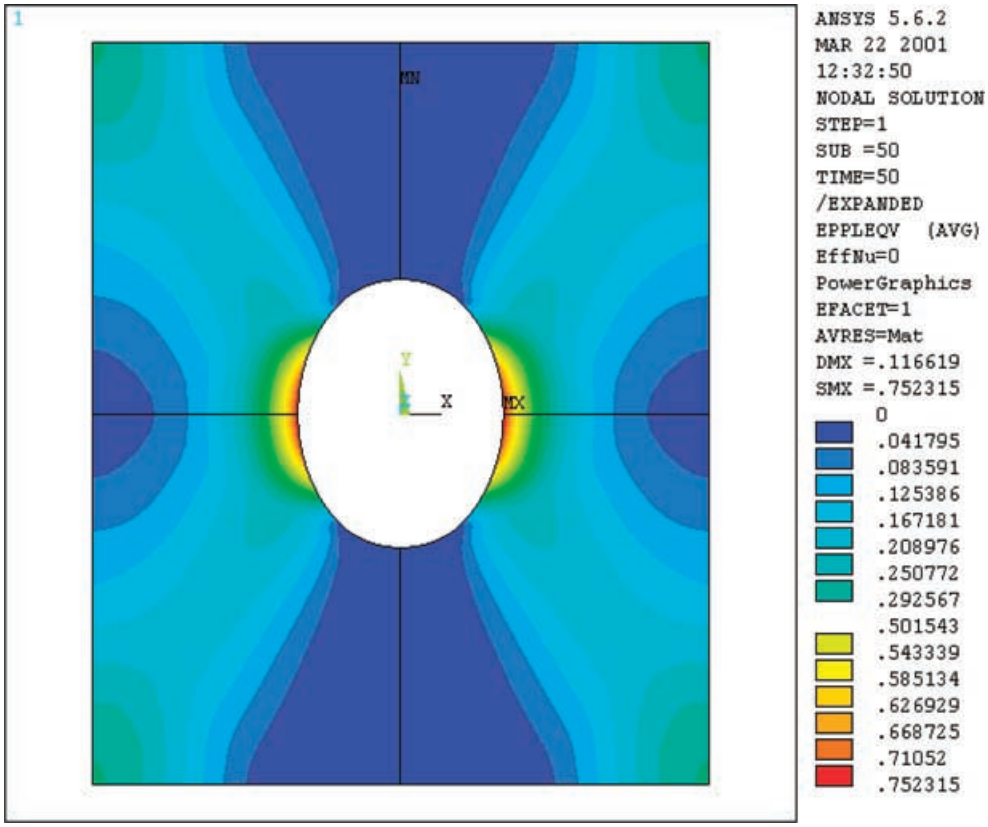

Fig. 12 Typical shape of plastic zones at link-up for low constraint.

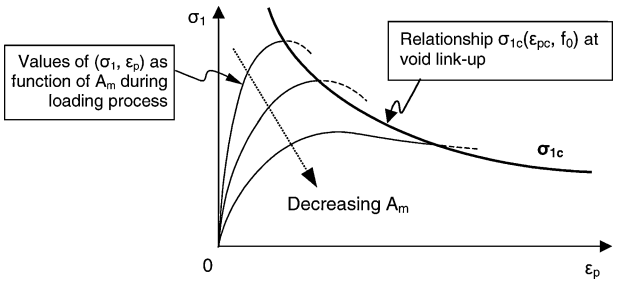

Fig. 13 Relationship between plastic limit-load stress σ_{1c} and critical effective plastic strain ε_{pc} for a specific f_0.

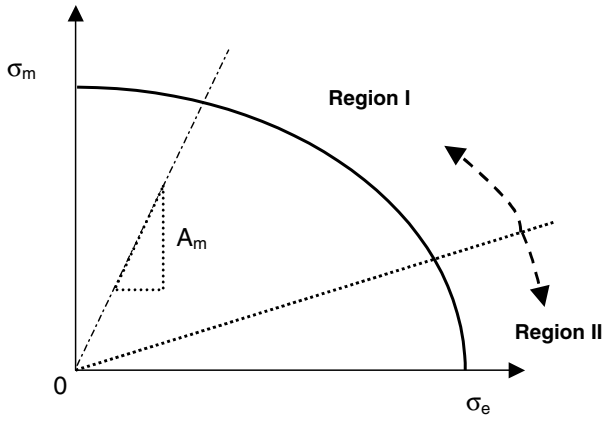

Fig. 14 Schematic of Regions I and II for (σ_m, σ_e) envelope with void volume fraction f_0.

trends observed by Thomason[17] for the plastic limit-load stress under low constraint conditions.

Also shown in Fig. 13 are typical 'loading' curves defining how the principal stress versus effective plastic strain relationship changes during the loading history under different levels of constraint A_m. Here, the intersection of each loading curve with the material curve defined by the function $\sigma_{1c}(\varepsilon_{pc}, f_0)$ corresponds to void link-up. By inspection of Fig. 13, there are two possibilities at void link-up. First, 'for high to moderate constraint A_m, the critical principal stress σ_{1c} corresponds to the maximum principal stress'. Second, 'for low constraint A_m, the critical principal stress σ_{1c} is less than the maximum principal stress in the loading history and link-up occurs at high levels of plastic strain and a principal stress σ_1 that is lower than the maximum value for this loading history'.

Consider a typical void link-up envelope function as shown in Fig. 14. Based on the discussion presented in the previous paragraphs, in terms of σ_m and σ_e the process of void link-up can be viewed as being composed of two regions. In Region I, which has high to moderate constraint A_m, the values of (σ_m, σ_e) correspond to plastic limit load conditions where the applied loading is a maximum at link-up. This region corresponds to void growth and coalescence due to a combination of mean stress and effective stress. In Region II, which has low constraint, the values of (σ_m, σ_e) correspond to high plastic strain and a principal stress that is below the maximum value for each loading history. Here, the damage due to increasing plastic strain at elevated effective stress and reduced constraint are sufficient to cause void coalescence and link-up at load levels that are below the maximum in the load history.

ADDITIONAL REMARKS

The simulations indicate that localization of plastic strain occurs along well-defined bands resulting in separation along these bands and void link-up, consistent with conditions corresponding to a maximum in effective stress and low constraint. If this statement is viewed in terms of macroscopic crack extension, then the presence of large plastic deformations in localized bands will initiate void growth from small secondary particles in these regions. This process will result in micro-void sheeting and link-up of the primary voids due to material separation along these bands.

In this regard, this work assumed a uniform distribution of spherical voids as the basis for the proposed failure criterion. However, real materials have variability in both secondary particle size and distribution that will affect the spatial distribution of void-coalescence sites. For example, recent studies for notches undergoing nominally mode I loading[28,29] have shown that void growth and coalescence in actual materials results in a microscopically tortuous, 3D circuit between particle bands. In this context, the authors believe that the proposed criterion $H(A_m, \sigma_e, f_0)$ is widely applicable because the spatial dimensions associated with typical secondary particle bands (e.g., size and spacing) are much smaller than the crack tip plastic zone associated with ductile crack growth. Here, f_0 in (4) is appropriately interpreted as an averaged void/particle volume fraction for the material.

The large distortion and void collapse observed in this work under low levels of constraint are consistent with previous observations,[17] providing additional evidence which indicates that void link-up is not related to the current void volume fraction used in dilatational plastic models that predict ductile fracture.[14–16] Rather, this work indicates that the inclusion of the effect of mean stress, σ_m, is necessary so that the critical conditions giving rise to micro-void coalescence[30,31] and, hence, ductile crack extension can be properly modelled.

However, in contrast to previous studies that focused on modelling of the void and ligament conditions at void-link-up, the enclosed study focuses on relating link-up conditions to the average response in the unit cell. Because the envelope function for each f_0 'can be interpreted in terms of a maximum effective stress criterion under a

constant level of constraint', it is conceptually possible to construct each envelope by performing a series of constant constraint experiments and determining the quantities (σ_m, σ_e) at the onset of void link-up, where (σ_m, σ_e) are 'continuum/average' quantities.

Because the ability to perform local, constraint-controlled experiments on specific voids in common structural materials is virtually impossible, the most obvious goal of this work is to utilize the unit-cell results and develop a physically sound, macroscopic, three-dimensional, ductile fracture criterion to predict ductile crack extension under general crack tip conditions. As an example, impurities in metallic alloys have been shown to be primary void initiation sites (e.g., commercial aluminium 2024-T3 contains up to 3.5% impurities by volume fraction) during stable crack extension. Because void growth is the established mechanism for crack extension in such material systems, and the initial volume fraction of impurities with weak interfaces is a reasonable estimate for f_0, the void link-up relationship $H(A_m, \sigma_e, f_0)$ indicates that $\sigma_e = \sigma_e(A_m, f_0)$ at the onset of crack extension. Furthermore, because the crack opening displacement (COD)[4,32–35] at any position behind the crack tip is the integrated effect of the elastic–plastic crack tip strain fields and $\varepsilon_p(\sigma_e(A_m, f_0))$, in regions where plastic deformation is dominant, then a viable COD fracture criterion that is consistent with the void link-up concepts outlined in this work is COD(A_m; f_0). Here, it is expected that the critical value of COD will decrease with increasing constraint.

Finally, with regard to the potential range of applicability of the proposed criteria, it is noted that deformation in the crack tip region of most ductile materials is much larger than that required for void nucleation, especially around large secondary particles. In such cases, exclusion of the void nucleation process will have minimal influence on the material failure event.

Acknowledgements

The authors gratefully acknowledge the financial support from the Air Force Research Laboratory (contract no. 00-3210-27-1) and from NASA (grant no. NCC5-174). In addition, the authors wish to thank Major Scott Fawaz, US Air Force Academy, and Dr. James Harter, US Air Force Research Laboratory, for their technical support throughout this effort.

REFERENCES

1 Rice, J. R. (1968) A path independent integral and the approximate analysis of strain concentration by notches and cracks. *J. Appl. Mech*. **35**, 379–386.
2 Hutchinson, J. W. (1968) Singular behavior at the end of a tensile crack in a hardening material. *J. Mech. Phys. Solids* **16**, 13–31.
3 Rice, J. R. and Rosengren, G. F. (1968) Plane strain deformation near a crack tip in a power law hardening material. *J. Mech. Phys. Solids* **16**, 1–12.
4 Sutton, M. A., Deng, X., Ma, F., Newman, J. C., Jr. and James, M. (2000) Development and application of a COD-based mixed mode fracture criterion. *Int. J. Solids Struct.* **37**, 3591–3618.
5 Chao, Y. J., Yang, S. and Sutton, M. A. (1994) On the fracture of solids characterized by one or two parameters: Theory and practice. High order asymptotic crack tip fields in a power law hardening material. *J. Mech. Phys. Solids* **42**, 629–647.
6 Gurson, A. L. (1977) Continuum theory of ductile rupture by void nucleation and growth, Part I: Yield criteria and flow rules for porous ductile media. *J. Engng Mater. Tech*. **99**, 2–15.
7 Needleman, A. and Tvergaard, V. (1984) An analysis of ductile rupture in notched bars. *J. Mech. Phys. Solids* **32**, 461–490.
8 Marin, E. B. (1993) A critical study of finite strain porous inelasticity. Ph.D. Thesis, Mechanical Engineering Department, Georgia Institute of Technology.
9 Marin, E. B. and McDowell, D. L. (1997) A semiimplicit integration scheme for rate-dependent and rate-independent plasticity. *Comput. Struct*. **63**, 579–600.
10 Xia, L. and Shih, C. F. (1995a) Ductile crack growth—I. A numerical study using computational cells with microstructurally-based length scales. *J. Mech. Phys. Solids* **43**, 233–259.
11 Xia, L. and Shih, C. F. (1995b) Ductile crack growth—II. Void nucleation and geometry effects on microscopic fracture behavior. *J. Mech. Phys. Solids* **43**, 1953–1981.
12 Xia, L. and Shih, C. F. (1996) Ductile crack growth—III. Transition to cleavage incorporating statistics. *J. Mech. Phys. Solids* **44**, 603–639.
13 Koppenhoefer, K. C. and Dodds, R. H., Jr. (1998) Ductile crack growth in pre-cracked CVN specimens: numerical studies. *Nucl. Engng Des*. **180**, 221–241.
14 Tvergaard, V. (1981) The influence of voids on shear band instabilities under plane strain conditions. *Int. J. Fract*. **17**, 389–407.
15 Tvergaard, V. (1987) Effect of yield surface curvature and void nucleation on plastic flow localization. *J. Mech. Phys. Solids* **35**, 43–60.
16 Tvergaard, V. and Needleman, A. (1984) Analysis of the cup-cone fracture in a round tensile bar. *Acta Metall*. **32**, 157–169.
17 Thomason, P. F. (1998) A view on ductile-fracture modelling. *Fatigue Fract. Engng Mater*. **21**, 1105–1122.
18 Pardoen, T. and Hutchinson, J. W. (2000) An extended model for void growth and coalescence. *J. Mech. Phys. Solids* **48**, 2467–2512.
19 Gologanu, M., Leblond, J.-B., Perrin, G. and Devaux, J. (1997) Recent extensions of Gurson's model for porous ductile metals. In: *Continuum Micromechanics* (Edited by P. Suquet), CISM courses and Lectures No. 377. Springer, New York.
20 Gologanu, M., Leblond, J.-B., Perrin, G. and Devaux, J. (2001a) Theoretical models for void coalescence in porous ductile solids, I. Coalescence 'in layers'. *Int. J. Solids Struct*. **38**, 5581–5594.
21 Gologanu, M., Leblond, J.-B. and Devaux, J. (2001b) Theoretical models for void coalescence in porous ductile solids, II. Coalescence 'in columns'. *Int. J. Solids Struct*. **38**, 5595–5604.
22 Rice, J. R. and Tracey, D. M. (1969) On the ductile enlargement of voids in triaxial stress fields. *J. Mech. Phys. Solids* **17**, 201–217.

23 Hancock, J. W. and Mackenzie, A. C. (1976) On the mechanisms of ductile failure in high-strength steels subjected to multi-axial stress-states. *J. Mech. Phys. Solids* **24**, 147–169.
24 Walsh, J. A., Jata, K. V. and Starke, E. A., Jr. (1989) The influence of Mn dispersoid content and stress state on ductile fracture of 2134 type Al alloys. *Acta Metall*. **37**, 2861–2871.
25 Gao, X., Shih, C. F., Tvergaard, V. and Needleman, A. (1996) Constraint effects on the ductile-brittle transition in small scale yielding. *J. Mech. Phys. Solids* **44**, 1255–1282.
26 Kuna, M. and Sun, D. Z. (1996) Three-dimensional cell model analyses of void growth in ductile materials. *Int. J. Fract*. **81**, 235–258.
27 Bishop, J. F. W. and Hill, R. A. (1951) theory of the plastic distortion of a polycrystalline aggregate under combined stresses. *Phil. Mag*. **42**, 414–427.
28 Everett, R. K., Simmonds, K. E. and Geltmacher, A. B. (2001) Spatial distribution of voids in HY-100 steel by X-ray tomography. *Scr. Mater*. **44**, 165–169.
29 Everett, R. K. and Geltmacher, A. B. (1999) Spatial distribution of MnS inclusions in HY-100 steel. *Scr. Mater.* **40**, 567–571.
30 Thomason, P. F. (1985) Three-dimensional models for the plastic limit loads at incipient failure of the intervoid matrix in ductile porous solids. *Acta Met*. **33**, 1079–1086.
31 Thomason, P. F. (1985) A three-dimensional model for ductile fracture by the growth and coalescence of microvoids. *Acta Met*. **33**, 1087–1095.
32 Han, G., Sutton, M. A. and Chao, Y. J. (1994) A study of stationary crack tip deformation fields in thin sheets by computer vision. *Exp. Mech*. **34**, 357–369.
33 Dawicke, D. S. and Sutton, M. A. (1994) CTOA and crack tunneling measurements in thin sheet 2024-T3 aluminium alloy. *Exp. Mech*. **34**, 357–369.
34 Amstutz, B. E., Sutton, M. A. and Dawicke, D. S. (1995) Experimental study of mixed mode I/II stable crack growth in thin 2024-T3 aluminium. *Fatigue Fract*. **26;** ASTM STP 1256, 256–273.
35 Ma, F., Deng, X., Sutton, M. A. and Newman, J. C., Jr. (1999) A CTOD-Based Mixed Mode Fracture Criterion. *Mixed Mode Crack Behavior*, ASTM STP 1359, 86–110.

APPENDIX

The typical relationship between the critical effective plastic strain ε_{pc} and the stress constraint A_m (Fig. 1) indicates that, for a specified value of ε_{pc}, there exists a corresponding level of A_m at which ductile failure will occur. On the other hand, multiple stress states (σ_m, σ_e) in a unit cell model can lead to the same effective plastic strain value ε_p in the model. Thus, a σ_m–σ_e curve can be constructed for each specified value of ε_p, as shown in Fig. A1.

Suppose that each curve shown in Fig. A1 is a compilation of values (σ_m, σ_e) at which 'link-up' occurs for an initial void volume fraction f_0 and a specified level of ε_p, where $\varepsilon_p{}^1 < \varepsilon_p{}^2 < \varepsilon_p{}^3 < \varepsilon_p{}^4$ is assumed for convenience. Based on the premise that a unique relationship exists between critical plastic strain and stress constraint, only one point (σ_m, σ_e) on each curve ε_p^i $(i = 1, 2, 3, 4)$ corresponds to the actual link-up of voids.

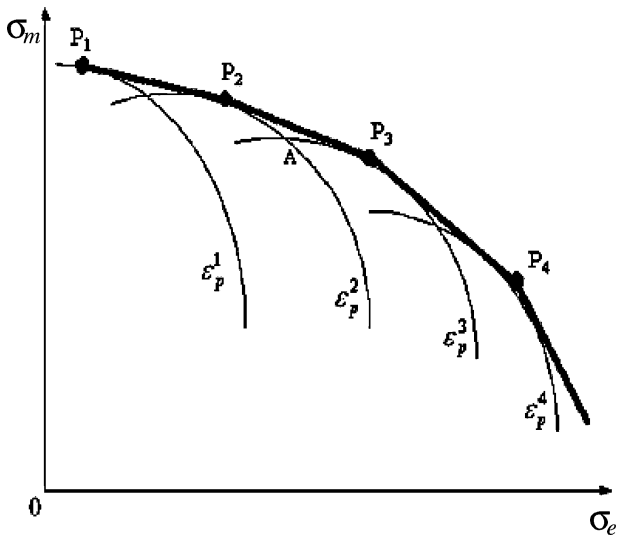

Fig. A1 Schematic for determining (σ_m, σ_e) at failure initiation.

An outer envelope is shown in Fig. A1, and each curve is tangent to the envelope at one point; tangent points shown in Fig. A1 are P_1, P_2, P_3 and P_4. If a monotonic relationship exists between ε_{pc} and constraint σ_m/σ_e then it is clear that the outer envelope of points represents the locus of values for (σ_m, σ_e) at which link-up has occurred. Thus, for each initial void volume fraction f_0, the envelope function ENV is the least upper bound (LUB) of the functional relationships ε_p^i (σ_m, σ_e) obtained from the numerical simulations, that is,

$$\mathrm{ENV}(\sigma_m, \sigma_e) = \mathrm{LUB}\{\varepsilon_p^i(\sigma_m, \sigma_e)\}. \tag{A.1}$$

It is worth noting that it is not possible for a point, (σ_m, σ_e), on the envelope to be at the intersection of two effective plastic strain curves, because there would exist two values of the effective plastic strain at link-up that correspond to the same ratio σ_m/σ_e, in conflict with the fundamental hypothesis that there exists a one-to-one relationship between ε_{pc} and the macroscopic stress constraint A_m. Hence, based on Eq. (A.1), it is concluded that there exists a unique functional relationship $H(\sigma_e, A_m, f_0)$ at failure initiation.

On the other hand, it can also be shown that 'the stress states given by the envelope in Fig. A1 are consistent with a maximum effective stress failure criterion at constant levels of constraint'. To demonstrate this assertion, consider the construction in Fig. A2 and suppose that P_i is an arbitrary point on the envelope. Then the stress constraint at point P_i is $A_m^{P_i} = (\frac{\sigma_m}{\sigma_e})|_{P_i} = \tan(\alpha)$, and the corresponding effective plastic strain contour value is $\varepsilon_p^{P_i}$. Let ε_p^A and ε_p^B be two selected values of the effective plastic strain so that

$$\varepsilon_p^A < \varepsilon_p^{P_i} \quad \text{and} \quad \varepsilon_p^B > \varepsilon_p^{P_i}. \tag{A.2}$$

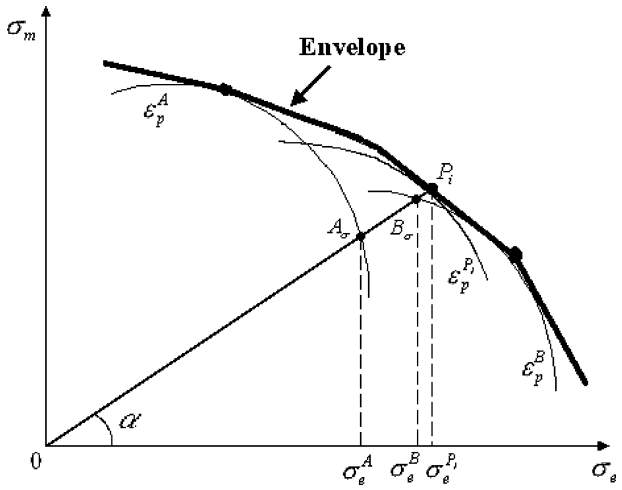

Fig. A2 Illustration of basis for maximum effective stress criterion.

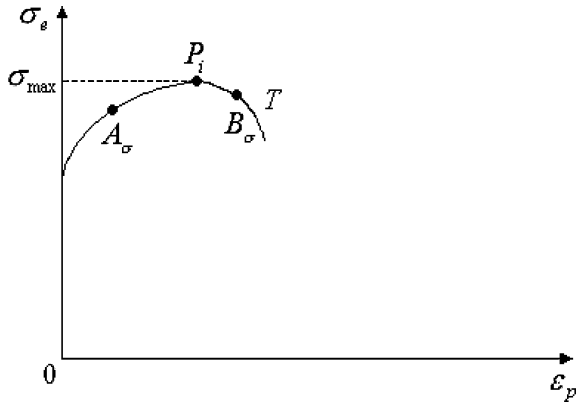

Fig. A3 Link-up stress under a constant stress constraint loading.

The line $\bar{OP}_i$ intersects with curves ε_p^A and ε_p^B at points A_σ and B_σ, respectively. The effective stresses σ_e^A, σ_e^B and $\sigma_e^{P_i}$ correspond to the points A_σ, B_σ and P_i, respectively, and it is clear that

$$\sigma_e^A < \sigma_e^{P_i} \quad \text{and} \quad \sigma_e^B < \sigma_e^{P_i}. \tag{A.3}$$

From Eqs (A.2) and (A.3), the effective stress corresponding to an arbitrary effective plastic strain is always less than the effective stress at point P_i. In other words, 'point P_i corresponds to the locus of values (σ_m, σ_e) where the effective stress is a maximum in the curve of effective stress versus effective plastic strain under constant stress constraint loading conditions'.

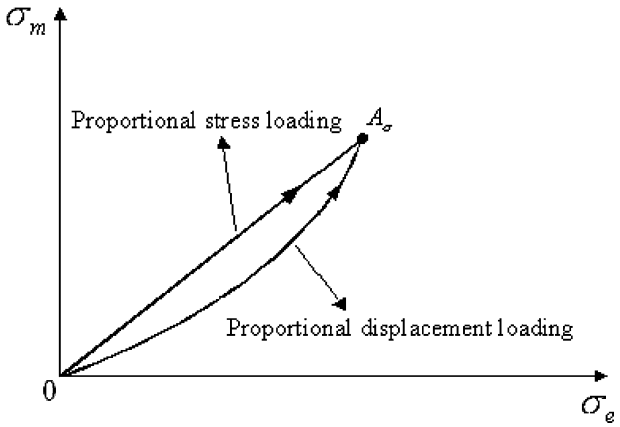

Fig. A4 Illustration of the loading history assumption.

Figure A3 shows a typical constant stress constraint loading history, with constraint $A_m = (\frac{\sigma_m}{\sigma_e})|_{P_i}$ where A_σ, B_σ and P_i are three stress states in the same constant-constraint loading history. Thus, the corresponding effective stress along a constant constraint loading history is always smaller than that at point P_i. In other words, 'point P_i is always at the position where the effective stress reaches its maximum in the curve of effective stress versus effective plastic strain'.

With regard to the stress history shown in Fig. A3, three points are noted here. First, because $\varepsilon_p^A < \varepsilon_p^{P_i} < \varepsilon_p^B$ during the monotonic loading process, the temporal order corresponding to loading point A_σ, B_σ and P_i is clearly

$$t_A < t_{P_i} < t_B. \tag{A.4}$$

Second, it is noted that an underlying hypothesis for the foregoing development is that 'the effective plastic strain under a proportional displacement loading to point A_σ is equal to the effective plastic strain under a proportional stress loading to point' A_σ. This is shown in Fig. A4, where σ_m and σ_e are the loading variables.

Third, if one assumes that there exists a unique functional relationship $H(\sigma_e, A_m, f_0)$ at void link-up, then the process shown in Figs A1 and A2 implies that there also exists a unique functional relationship $F(\varepsilon_{pc}, A_m, f_0)$ that is similar to the form shown in Fig. 1.